Soft matter: from shapes to forces on the nanoscale

Derek Y. C. Chan,†*[ab] Ofer Manor,[a] Jason N. Connor‡[c] and Roger G. Horn[c]

Received 22nd August 2007, Accepted 14th November 2007
First published as an Advance Article on the web 8th January 2008
DOI: 10.1039/b712924f

Soft matter deforms in response to imposed external forces. Here we demonstrate how dynamic surface forces are linked to far-field deformations. This offers a new paradigm for determining forces between soft particles in colloidal systems. The particular example we use to illustrate this concept is that of a fluid drop interacting with a solid wall through hydrodynamic drainage flow coupled with repulsive or attractive dissimilar electrical double layer interactions. The force can be deduced from a simple analysis of the drop surface geometry outside the interaction zone.

Colloidal interactions between solid bodies are reasonably well understood, thanks in large part to direct measurement techniques. However, the interactions between soft objects such as fluid drops or bubbles have not been investigated so extensively. Measurements of forces between particles require recording particle displacements in an applied force field. In the surface force apparatus (SFA)[1] or the atomic force microscope (AFM)[2] the applied field is provided by a calibrated mechanical spring; in total internal reflection microscopy (TIRM)[3] gravity is the external field; while in the optical tweezers technique,[4] the external field is of electromagnetic origin. It is relatively straightforward to deduce the force between rigid bodies from recorded particle displacements in the known external force field. For interactions involving particles of soft matter, the particles themselves deform during the course of the interaction and so the relationship between force and displacement becomes more complex. The changing geometry of the soft body is coupled to the force in a mutually-consistent way, and both can vary with separation and possibly with time.

The total force between particles of soft matter is encoded in the geometry of the deformations. Therefore, it should be possible to deduce interaction forces by analysing the particle deformations without the need to impose an external force field provided by a mechanical spring, gravity or applied electromagnetic field. Here we demonstrate and quantify the connection between geometry and the interaction force involving deformable drops in solution. The generalisation to other soft matter is feasible if we know the mechanical equation of state of the material. The approach is based on a simple analysis of recent high-resolution real-time observations of dynamic deformations of a charged deformable mercury–aqueous electrolyte interface due to an approaching molecularly smooth mica plate.[5,6] The electrical double layer interaction between the mica and the mercury can be tuned to give a range of repulsive interactions that lead to the formation of stable aqueous films of different equilibrium thicknesses between the mercury and the approaching mica plate, or attractive interactions that result in the coalescence of the mercury interface onto the mica surface during approach. Our analysis is capable of giving the time- and distance-dependent dynamic force of interaction that has contributions from hydrodynamic effects in addition to repulsive or attractive electrical double layer forces.

The key experimental information comes from observing dynamic deformations of the mercury–electrolyte interface on a protuberant drop at the end of a sealed, constant volume, capillary tube that are induced by driving a molecularly smooth mica plate towards the interface (Fig. 3, inset). Analysis of video recordings of fringes of equal chromatic order (FECO) corresponding to real-time axisymmetric deformations of the mercury interface gives sub-nanometre resolution of the mica–mercury separation, $h(r,t)$. Representative data are presented in Fig. 1, with particular focus on an extended

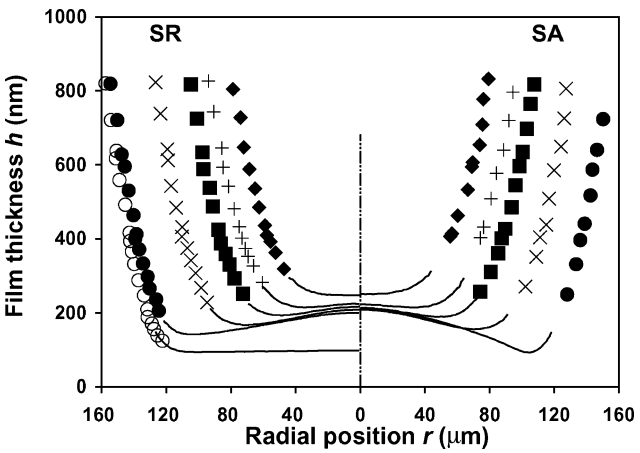

Fig. 1 Examples of measured thicknesses $h(r,t)$ of the axisymmetric aqueous film between the mica and the mercury at various times. The diagram is split so that the left hand side shows data obtained under strongly repulsive (SR) disjoining pressure conditions while the right-hand side shows data for strongly attractive (SA) disjoining pressure conditions – the thickness profile is axisymmetric. The reference time $t = 0$ is defined to be the instant when the curvature of $h(r,t)$ at $r = 0$ changes sign. Symbols correspond to film thicknesses at large r values at $t = 0.02$ s (◆), 0.10 s (+), 0.18 s (■), 0.34 s (×), 0.62 s (●), and 9.62 s (○). The thin solid lines represent previously published data analysed at smaller r for the same conditions.[6] Due to strong electrostatic attractions in the SA case, the mercury interface collapsed onto the mica after 0.62 s.

[a]*Particulate Fluids Processing Centre, Department of Mathematics and Statistics, The University of Melbourne, Parkville, VIC, 3010, Australia. E-mail: D.Chan@unimelb.edu.au; O.Manor@pgrad.unimelb.edu.au; Fax: +61 3 8344 4599; Tel: +61 3 8344 5556*

[b]*Department of Mathematics, National University of Singapore, 117543, Singapore. E-mail: matchand@nus.edu.sg; Fax: +65 6779 5452; Tel: +65 9759 3954*

[c]*Ian Wark Research Institute, University of South Australia, Mawson Lakes, South Australia, 5095, Australia. E-mail: Roger.Horn@unisa.edu.au; Fax: +61 8 8302 3683; Tel: +61 8 8302 3596*

† D. C. is a Visiting Professor at the National University of Singapore and the A-STAR Institute of High Performance Computing, Singapore.

‡ *Current address*: PELM Centre, Central Queensland University, Gladstone, Queensland 4680, Australia. E-mail: j.n.connor@cqu.edu.au; Fax: +61 7 4970 7608; Tel: +61 7 4970 7338.

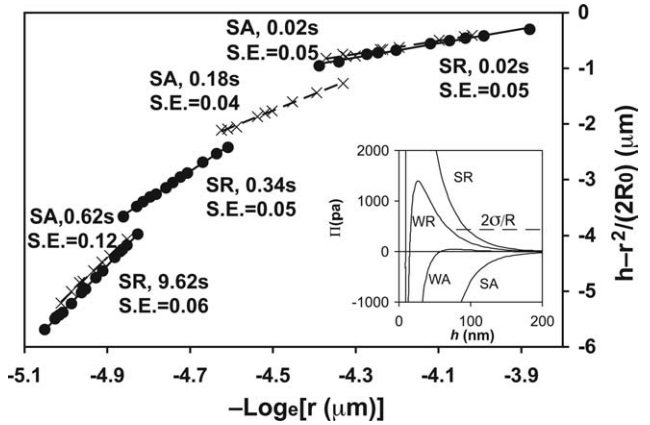

Fig. 2 Examples of linear regression using eqn (6) to fit the large r film profiles given as symbols in Fig. 1 by plotting $[h(r,t) - r^2/(2R_0)]$ against $\log_e(r)$ for which $F(t)/(2\pi\sigma)$ is the slope of the SR (■) and SA (+) data. Datasets at selected times as indicated correspond to strongly repulsive (SR) and strongly attractive (SA) disjoining pressures $\Pi(h)$ (inset). The standard errors (S. E.) of the slope of the linear regression lines are also shown. Inset: disjoining pressures for the mercury with various surface potentials: strongly repulsive (SR, −492 mV), weakly repulsive (WR, −52 mV), weakly attractive (WA, −12 mV) and strongly attractive (SA, +408 mV) due to electrical double layer interactions with the mica surface (−100 mV) at 0.1 mM 1 : 1 electrolyte concentration.[6]

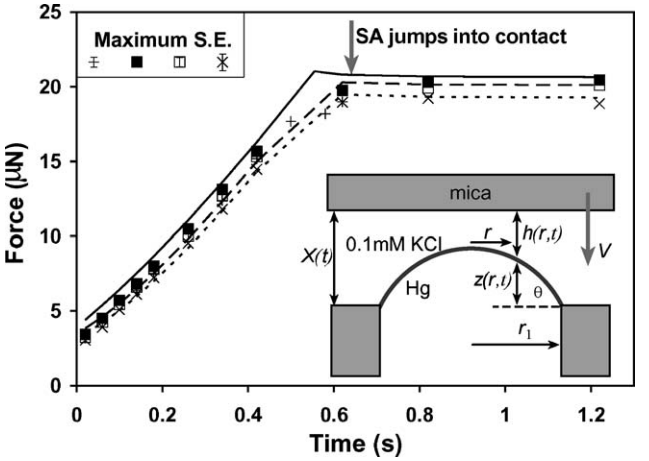

Fig. 3 The force at short times for SR (■, —), WR (□, – –), WA (×, ···) and SA (+) interactions. Symbols represent data obtained by fitting eqn (6) to the large r form of the experimental film thickness as indicated in Fig. 2, and corresponding lines are results obtained by the numerical solution of eqn (1)–(4).[9] The mica is driven at a nominal constant velocity of 24 μm s^{-1} towards the mercury for 0.56 s. For the SA case, the film collapsed after 0.62 s. The maximum standard errors (S. E.) of the force for each case are as indicated. The S. E. of the force is obtained from the S. E. of the slope in Fig. 1. The uncertainty in the time step is 0.02 s which is half the duration of a single video frame. Inset: schematic diagram of the experimental apparatus where a molecularly smooth mica plate is driven towards a protuberant mercury drop located at the end of a sealed capillary tube of radius $r_1 = 1.5$ mm. The normal to the mica plate is oriented parallel to the capillary axis, which is vertical. The unperturbed mercury drop has an apex radius of curvature $R_0 = 1.9$ mm and makes a contact angle $\theta = 55°$ with the capillary tube.

range of h and r beyond that which has been presented previously.[6] Effects of different repulsive and attractive disjoining pressures due to electrical double layer interactions shown in the inset of Fig. 2 have been investigated. The forms of these disjoining pressures are determined by setting the bias voltage on the mercury.[5,6]

A model to describe the space–time evolution of the deforming interface in this experimental system has been developed elsewhere.[7–9] It gives very good agreement with force measurements between deformable drops[10] as well as various mechanical and electrical perturbations of deformable interfaces.[11] The thickness, $h(r,t)$ (∼100 nm) of the aqueous film between the mica and the mercury is much smaller than the undistorted drop apex radius of curvature, R_0 (∼2 mm), so this system is in the regime where Stokes flow and Reynolds lubrication theory are appropriate for describing the evolution of the aqueous film with constant shear viscosity μ as the Reynolds number based on the film thickness and mica velocity is $<10^{-6}$. This gives the drainage equation for the film thickness $h(r,t)$

$$\frac{\partial h}{\partial t} = \frac{1}{12\mu r}\frac{\partial}{\partial r}\left(r\,h^3\,\frac{\partial p}{\partial r}\right) \tag{1}$$

where $p(r,t)$ is the hydrodynamic pressure relative to the bulk fluid. The shape function $z(r,t) = X(t) - h(r,t)$ of the mercury–electrolyte interface (see Fig. 3, inset) with constant interfacial tension, σ, obeys the Young–Laplace equation:

$$\frac{\sigma}{r}\frac{\partial}{\partial r}\left(\frac{r(\partial z/\partial r)}{\left[1+(\partial z/\partial r)^2\right]^{1/2}}\right) = (p+\Pi) - \frac{2\sigma}{R} \tag{2}$$

where $(2\sigma/R)$ is the Laplace pressure of the drop and $\Pi(h(r,t))$ is the disjoining pressure that arises from electrical double layer interactions between the dissimilarly charged mica and mercury surfaces. The analysis assumes no direct coupling between p and Π, in other words it does not include possible electrokinetic effects. This assumption is justified *a posteriori* below. The non-linear Poisson–Boltzmann theory, has been shown to give an accurate description of $\Pi(h)$, which is due to electrical double interaction for this system.[5] The total instantaneous force of interaction, between the mica and the deformable mercury surface, is given in terms of the dynamic disjoining pressure $(p + \Pi)$

$$F(t) = 2\pi\int_0^\infty [p(r,t) + \Pi(h(r,t))]\,r\,\mathrm{d}r \tag{3}$$

Details of the evolution of the film between the mica and the mercury interface can be obtained by numerical solution of the governing eqn (1) and (2) in a domain: $0 < r < r_{max}$ with the initial condition: $h(r,t_{init}) = h_0 + r^2/(2R_0)$ and the boundary condition at $r = r_{max}$ that reflects the constant volume constraint of the mercury drop.[9] This boundary condition depends on the contact angle, θ, of the mercury drop at the capillary and is based on the justified assumption that the three phase contact line at the base of the mercury drop is pinned at the radius of the capillary, r_1 (see definitions in Fig. 3 inset)[7]

$$\frac{\partial h}{\partial t} = \frac{\mathrm{d}X(t)}{\mathrm{d}t} - \frac{1}{2\pi\sigma}\left[1+\frac{1}{2}\log\left(\frac{1+\cos\theta}{1-\cos\theta}\right)+\log\left(\frac{r_{max}}{2R_0}\right)\right]\frac{\mathrm{d}F}{\mathrm{d}t},\quad \text{at } r = r_{max} \tag{4}$$

If instead, the drop rested on a smooth substrate where the three phase contact line were free to move to preserve the equilibrium

contact angle, a slightly different expression would appear in the pre-factor of (dF/dt).[7] In practice, the value of r_{max} is chosen to be sufficiently large where effects due to disjoining pressure $\Pi(h(r,t))$ for $r > r_{max}$ are negligible, but r_{max} is still small compared to the undistorted drop apex radius of curvature, R_0. Numerical results should not depend on the precise value of r_{max}. A choice of $r_{max}/(Ca^{1/4}\ R_0) \sim 10$–15, where $Ca = (\mu V/\sigma) \sim 10^{-7}$ is the capillary number, gives a good balance between speed of computation and at least 7 significant figures of computational precision.[7] In the present case, $r_{max} \sim 300$–500 μm. Comparison between theory and experiment then requires the numerical solution of the sytem of differential-algebraic eqn (1)–(4) to match the film profile $h(r,t)$ and then compute the force from eqn (3).[9]

A novel way to obtain the force that circumvents such numerical computation can be found from considering the far field shape of the deformed drop outside the film. For $r \ll R_0$, the inner solution for eqn (2) can be derived by first omitting the small term $(\partial z/\partial r)^2$ in the denominator. The resulting equation can then be integrated twice to give[12]

$$z(r,t) = z(0,t) - \frac{r^2}{2R} + \frac{1}{\sigma}\int_0^r dr'\ r'\ (p+\Pi)\log(r/r') \qquad (5)$$

When r exceeds the range over which the dynamic disjoining pressure $p + \Pi$ is significant, the upper limit of the integral can be replaced by infinity and, using eqn (3), the limiting form of the film thickness $h(r,t) = X(t) - z(r,t)$ is

$$h(r,t) \cong \left\{ c(t) + \frac{r^2}{2R_0} + \frac{F(t)}{2\pi\sigma}\log(r) \right\}\left[1 + O\left(\frac{F}{\sigma R_0}\right)\right] \qquad (6)$$

where $c(t)$ is independent of r. This is our key result, which follows from the small deformation expression, for the Laplace radius[13]

$$R \approx R_0\left[1 - \frac{F}{2\pi\sigma\ R_0\ (1-\cos\theta)} + O\left(\frac{F}{\sigma R_0}\right)^2\right] \qquad (7)$$

Eqn (6) holds in the far field region of r outside the film where both the hydrodynamic and disjoining pressures are negligible but where r is still small compared to the drop radius. For the experimental situations considered here, the condition $F/(\sigma R_0) < 10^{-2}$ holds, so the profile in eqn (6) has a functional form that comprises a quadratic term ($\sim r^2$) plus a term proportional to $\log(r)$ that has the dynamic force $F(t)$ as the pre-factor. Therefore by fitting eqn (6) to experimental surface profiles in the large r region of the film, the dynamic force can be obtained without the need to solve eqn (1)–(3) numerically to match the film profile as in earlier work.[9]

To demonstrate the utility of this approach, we measured surface profiles of the mercury interface where the mica was driven at a constant velocity, $dX/dt = -V = -24\ \mu m\ s^{-1}$, towards the mercury for 0.56 s and then was stopped. The results of fitting eqn (6) to film thickness at large r for the two extremes cases of disjoining pressures that we call strongly attractive (SA) and strongly repulsive (SR) are shown in Fig. 2 at selected time values. We use previously unpublished data shown as symbols in Fig. 1 that are film thicknesses at positions far from the center of the film. The reference $t = 0$ is chosen to be the time when the curvature of the profile at $r = 0$ first changes sign.[6] For each time step, the corresponding force $F(t)$ is extracted from measured film thicknesses at large r by a linear regression of $[h(r,t) - r^2/(2R_0)]$ plotted against $\log_e(r)$. The accuracy of eqn (6) can be gauged from the representative fits shown in Fig. 2. The unknown constant $c(t)$ and the units of r do not affect the value of slope extracted from Fig. 2.

Note in particular that the method of using eqn (6) to obtain the dynamic time- and distance-dependent force only requires information about the instantaneous shape of the film in the large r region of the film. Details of the film geometry in the inner or central small r region, which may be more difficult to obtain experimentally, are not required. Furthermore since only the shape of the film, rather than the absolute value of the film thickness is needed, this approach is more tolerant of possible experimental uncertainties and may be suitable for studying collisions between emulsion drops.

We observe in Fig. 3 that during the initial 0.56 s, while the mica is being driven towards the mercury, the forces for the cases of strongly repulsive (SR), weakly repulsive (WR), weakly attractive (WA) and strongly attractive (SA) disjoining pressures due to electrical double layer interactions are all similar. In all cases, the dominant interaction during this time is the repulsive hydrodynamic pressure due to drainage of the thin aqueous film between the mica and the mercury.[9,14] The drainage phenomenon is coupled to deformations of the mercury–electrolyte interface under the restoring influence of surface tension. However, at $t \sim 0.62$ s, the aqueous film in the SA case became sufficiently thin to come under the strong attractive electrical double layer force, which caused the mercury to jump into contact with the mica and the aqueous film collapses.

The behaviour of the force after the mica has stopped reflects the way the aqueous films approach their final states under different cases of the disjoining pressure (Fig. 4). In the SR and the WR cases, the film will reach different equilibrium thicknesses h_{eq} as dictated by the balance of the Laplace pressure of the drop against the repulsive disjoining pressure: for SR $h_{eq} = 94$ nm and for WR $h_{eq} = 64$ nm.[6] However, for the WA case, the aqueous film eventually collapses

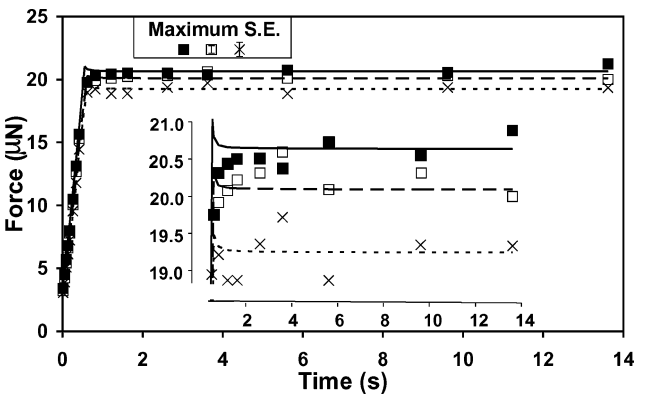

Fig. 4 The behaviour of the force at longer times for SR (■, —), WR (□, – –) and WA (×, ···) after the mica has stopped and the film drains to equilibrium thicknesses for the SR and WR cases. For the WA case, the film eventually collapses at around 18 s (not shown).[6] Symbols represent data obtained by fitting eqn (6) to the large r form of the experimental film thickness as indicated in Fig. 2 and corresponding lines are results obtained by the numerical solution of eqn (1)–(4).[9] The maximum standard errors (S. E.) of the force for each case are as indicated. Inset: details of the force between 18 μN and 21 μN. The overshoot in the calculated forces just after the mica stops is a numerical artefact due to the abrupt change of the mica velocity from 24 μm s^{-1} to zero over one integration time-step.

although it takes a long time (~18 s) doing so because the attractive disjoining pressure is weak and the film-thinning process continues to be dominated by hydrodynamic drainage effects that have a long time scale. In all three cases, after the mica stops, that is when $dX/dt = 0$, we expect $\partial h(r,t)/\partial t = 0$ at $r = r_{max}$ so that according to eqn (4) we see that the system will evolve towards various final states under a constant force regime, as reflected in Fig. 4. This constant force behaviour is a consequence of the fact that deformation of the mercury–electrolyte interface remains small on the length scale of the drop dimension so that the Laplace pressure of the drop remains essentially unchanged as the mica approaches the (slightly) deforming drop. After the mica stops, the radial extent of the deformed region remains constant which at constant Laplace pressure gives rise to a constant force. Furthermore, the value of the constant force is essentially the same regardless of the strength and sign of the double layer interaction (SR, WR or in the case of WA before the film finally collapses). These observations support the general conclusion that, the total force is determined simply and solely by the displacement $X(t)$ of the body of the drop with respect to the mica, regardless of how the force is mediated. And at low velocities considered here and film thickness large compared to the Debye length, electrokinetic effects such as electro-osmosis, appear not to be important over time scales of these experiments which are of the order seconds. This justifies the assumptions made in using eqn (1) and (2).

Note that while the total force remains constant after the mica has stopped moving with respect to the capillary holding the drop, the respective contributions of double layer force and hydrodynamic force continue to evolve with time as the system approach the final state configuration.[9,14] For the SR and WR cases which eventually approach an equilibrium film, the contribution from the hydrodynamic pressure will decay as the film approaches equilibrium. On the other hand, the contribution from the disjoining pressure due to electrical double layer interactions, which was small while the mica was being driven towards the mercury, progressively increases and replaces the decaying hydrodynamic pressure until eventually it is the only mechanism that maintains an equilibrium film.

By using a well controlled and high resolution experimental system with sub-nanometre resolution, we have demonstrated that the connection between shape and force on a deformable body can be exploited to extract accurately time-dependent forces from geometric analysis of deformations outside the region where detailed and complex interactions take place. While the present experimental system only requires a model with constant interfacial tension to capture its behaviour, the analysis that leads to eqn (6) will still carry through even if the interfacial tension is not constant in the inner interaction zone but has reached a constant value in the large r limit. This offers the exciting opportunity, for example, of using image capture and analysis to infer forces between interacting but freely moving drops in emulsions or between such drops and other interfaces.

Acknowledgments

This work has been supported in part by two Australian Research Council Special Research Centres: the Particulate Fluids Processing Centre at the University of Melbourne and the Particle and Material Interfaces Centre at the Ian Wark Research Institute, University of South Australia. O. M. is supported by a University of Melbourne International Research Scholarship.

References

1 J. N. Israelachvili and G. E. Adams, *J. Chem. Soc., Faraday Trans. 1*, 1978, **74**, 975.
2 W. A. Ducker, T. J. Senden and R. M. Pashley, *Langmuir*, 1992, **8**, 1831.
3 D. C. Prieve, *Adv. Colloid Interface Sci.*, 1999, **82**, 93.
4 A. Ashkin, J. M. Dziedzic, J. E. Bjorkholm and S. Chu, *Opt. Lett.*, 1986, **11**, 288.
5 J. N. Connor and R. G. Horn, *Langmuir*, 2001, **17**, 7194.
6 J. N. Connor and R. G. Horn, *Faraday Discuss.*, 2003, **123**, 193.
7 S. L. Carnie, D. Y. C. Chan, C. Lewis, R. Manica and R. R. Dagastine, *Langmuir*, 2005, **21**, 2912.
8 S. L. Carnie, D. Y. C. Chan and R. Manica, *ANZIAM J.*, 2005, **46**, C805.
9 R. Manica, J. N. Connor, S. L. Carnie, R. G. Horn and D. Y. C. Chan, *Langmuir*, 2007, **23**, 626.
10 R. R. Dagastine, R. Manica, S. L. Carnie, D. Y. C. Chan, G. W. Stevens and F. Grieser, *Science*, 2006, **313**, 210.
11 R. Manica, J. S. Connor, L. Y. Clasohm, S. L. Carnie, R. G. Horn and D. Y. C. Chan, *Langmuir*, 2007, DOI: 10.1021/la701562q.
12 D. Y. C. Chan, R. R. Dagastine and L. R. White, *J. Colloid Interface Sci.*, 2001, **236**, 141.
13 D. C. Bardos, *Surf. Sci.*, 2002, **517**, 157.
14 R. G. Horn, M. Asadullah and J. N. Connor, *Langmuir*, 2006, **22**, 2610.

